Oxalate-induced chronic kidney disease with its uremic and cardiovascular complications in C57BL/6 mice

Mulay, Shrikant Ramesh ; Eberhard, Jonathan Nicodemos ; Pfann, Victoria ; Marschner, Julian A ; Darisipudi, Murthy Narayana ; Daniel, Christoph ; Romoli, Simone ; Desai, Jyaysi ; Grigorescu, Melissa ; Kumar, Santosh V ; Rathkolb, Birgit ; Wolf, Eckhard ; de Angelis, Martin Hrabě ; Bäuerle, Tobias ; Dietel, Barbara ; Wagner, Carsten A ; Amann, Kerstin ; Eckardt, Kai-Uwe ; Aronson, Peter S ; Anders, Hans Joachim ; Knauf, Felix

Abstract: Chronic kidney disease (CKD) research is limited by the lack of convenient inducible models mimicking human CKD and its complications in experimental animals. We demonstrate that a soluble oxalate-rich diet induces stable stages of CKD in male and female C57BL/6 mice. Renal histology is characterized by tubular damage, remnant atubular glomeruli, interstitial inflammation, and fibrosis with the extent of tissue involvement depending on the duration of oxalate feeding. Expression profiling of markers and magnetic resonance imaging findings established to reflect inflammation and fibrosis parallel the histological changes. Within 3 weeks the mice reproducibly develop normochromic anemia, metabolic acidosis, hyperkalemia, FGF23 activation, hyperphosphatemia and hyperparathyroidism. In addition, the model is characterized by profound arterial hypertension as well as cardiac fibrosis that persist following the switch to a control diet. Together, this new model of inducible CKD overcomes a number of previous experimental limitations and should serve useful in research related to CKD and its complications.

DOI: https://doi.org/10.1152/ajprenal.00488.2015

Articles in PresS. Am J Physiol Renal Physiol (January 13, 2016). doi:10.1152/ajprenal.00488.2015

Oxalate-induced chronic kidney disease with its uremic and cardiovascular complications in C57BL/6 mice

Shrikant R. Mulay[1]*, Jonathan N. Eberhard[1]*, Victoria Pfann*[2], Julian A. Marschner[1], Murthy N. Darisipudi[2], Christoph Daniel[3], Simone Romoli[1], Jyaysi Desai[1], Melissa Grigorescu[1], Santhosh V. Kumar[1], Birgit Rathkolb[4,5], Eckhard Wolf[5], Martin Hrabě de Angelis[4,6,7], Tobias Bäuerle[8], Barbara Dietel[9], Carsten A. Wagner[10], Kerstin Amann[3], Kai-Uwe Eckardt[2], Peter S. Aronson[11], Hans Joachim Anders[1]*, Felix Knauf[2,11]*
*Indicates equal contribution

1 Medizinische Klinik und Poliklinik IV, Klinikum der Universität München, Munich, Germany
2 Department of Nephrology and Hypertension, Friedrich-Alexander-Universität Erlangen-Nürnberg (FAU), Erlangen, Germany
3 Department of Nephropathology, Friedrich-Alexander-Universität Erlangen-Nürnberg (FAU), Erlangen, Germany
4 German Mouse Clinic, Institute of Experimental Genetics, Helmholtz-Zentrum München, Neuherberg, Germany
5 Institute of Molecular Animal Breeding and Biotechnology, Gene Center, Ludwig-Maximilians-University München, Munich, Germany
6 Chair of Experimental Genetics, School of Life Science Weihenstephan, Technische Universität München, Freising, Germany
7 German Center for Diabetes Research (DZD), Neuherberg, Germany
8 Preclinical Imaging Platform Erlangen, Institute of Radiology, Friedrich-Alexander-Universität Erlangen-Nürnberg (FAU), Erlangen, Germany
9 Department of Cardiology, Friedrich-Alexander-Universität Erlangen-Nürnberg (FAU), Erlangen, Germany
10 Zurich Center for Integrative Human Physiology, Zurich, Switzerland
11 Department of Internal Medicine, Yale University School of Medicine, New Haven, Connecticut, USA

Number of text pages: 15, **Number of figures**: 7, **Number of tables:** 2,
Number of supplementary tables: 1,
Word count of abstract: 154; **of manuscript**: 3070
Short title: Oxalate-induced CKD mouse model

Corresponding author:
Felix Knauf, M.D.
Department of Nephrology and Hypertension
Friedrich-Alexander-Universität (FAU)
Universitätsklinikum Erlangen
Schwabachanlage 12
91054 Erlangen, Germany
Tel.: +49-9131-85-39572
Fax: +49-9131-85-39561
Email: Felix.Knauf@uk-erlangen.de

Abstract

Chronic kidney disease (CKD) research is limited by the lack of convenient inducible models mimicking human CKD and its complications in experimental animals. We demonstrate that a soluble oxalate-rich diet induces stable stages of CKD in male and female C57BL/6 mice. Renal histology is characterized by tubular damage, remnant atubular glomeruli, interstitial inflammation, and fibrosis with the extent of tissue involvement depending on the duration of oxalate feeding. Expression profiling of markers and magnetic resonance imaging findings established to reflect inflammation and fibrosis parallel the histological changes. Within 3 weeks the mice reproducibly develop normochromic anemia, metabolic acidosis, hyperkalemia, FGF23 activation, hyperphosphatemia and hyperparathyroidism. In addition, the model is characterized by profound arterial hypertension as well as cardiac fibrosis that persist following the switch to a control diet. Together, this new model of inducible CKD overcomes a number of previous experimental limitations and should serve useful in research related to CKD and its complications.

Key words: renal failure, oxalate, CKD-MBD, hypertension, cardiovascular

Introduction

Translational research in the area of chronic kidney disease (CKD) requires experimental models that (1) can be induced in C57BL/6 mice as it represents the most commonly used genetic background for gene manipulations, (2) reliably generate stable CKD, (3) result in CKD within a relatively short time to limit the burden for animals and reduce housing costs, (4) do not require surgery in order to minimize animal distress and the use of anesthetic drugs or pain killers with potentially confounding effects. In addition, an ideal model should (5) work in male and female mice with low inter-individual variability to allow sex-based comparisons in response to interventions and minimize animal use, (6) not reduce renal mass, which limits the tissue available for analysis, (7) reduce glomerular filtration rate (GFR) by more than 50% in order to allow detection of the changes in the clinical biomarkers plasma blood urea nitrogen (BUN) and creatinine, and (8) be associated with typical complications associated with CKD in humans, such as normochromic anemia, hyperphosphatemia, hyperparathyroidism, hyperkalemia, acidosis, hypertension, and cardiovascular disease. The present work reviews the most commonly used murine models of inducible CKD (1, 3, 12, 16) and contrasts them with a novel oxalate-induced model of stable CKD.

Methods

Animal studies and analytical methods

Male and female 8-12 week old gender-matched C57BL/6 mice were obtained from Charles River Laboratories (Sulzfeld, Germany), housed in groups of five mice in standard housing conditions with unlimited access to food and water. Oxalate diet was prepared by

adding 50 µmol/g sodium oxalate to a calcium-free standard diet (Ssniff, Soest, Germany) as previously described (15). Removal of calcium from the diet increases the amount of soluble oxalate available for absorption as previously shown (15). Oxalate- and calcium-free diet (control diet) was given for 3 days to eliminate any residual intestinal calcium before switching to high soluble oxalate diet and used after ending the oxalate feeding period. All experimental procedures were approved by the local government authorities.

Assessment of renal injury

Mice kidney sections of 2 µm were stained with periodic acid-Schiff (PAS) reagent. Tubular injury was scored by assessing the percentage of necrotic tubules and presence of tubular casts. F4/80+ve positive macrophages, CD3+ve T cells (both Serotec, Oxford, UK) were identified by immunostaining and were counted in 15 high power fields (hpf) per section using Image J software. Similar approach was also used to quantify Silver stains. Fibrotic areas were identified by Silver stain, Masson Trichrome stain & Collagen 1a1 and were quantified using Image J software. Serial sections of the kidney were stained with Tetragonolobus lectin to observe atubular glomeruli. All assessments were performed by an observer blinded to the experimental condition.

RNA preparation and real-time quantitative -PCR

Total RNA was isolated from kidneys using a Qiagen RNA extraction kit (Qiagen, Germany) following the manufacturer's instructions. After quantification RNA quality was assessed using agarose gels. From isolated RNA, cDNA was prepared using reverse transcriptase (Superscript II)

(Invitrogen, USA). Real time RT-PCR was performed using SYBRGreen PCR master mix and was analyzed with a Light Cycler 480 (Roche, Germany). All gene expression values were normalized using 18s RNA as a house keeping gene. All primers used for amplification were from Metabion (Martinsried, Germany) and are listed in Table 1.

Hematological analysis

Hematological analysis was performed using prefilled Sysmex capillary tubes (Sysmex Deutschland GmbH, Norderstedt, Germany). An aliquot of 50µl EDTA-blood was determined by using a 50µl end-to-end capillary and was diluted 1:5 in 200µl prefilled Sysmex Cellpack buffer. Diluted samples were stored at room temperature until analysis. Complete peripheral blood counts, differential leukocyte counts and reticulocyte counts were determined with a Sysmex XT2000iV hematology analyzer (Sysmex Deutschland GmbH, Norderstedt, Germany) in the "capillary blood" mode using the option "CBC DIFF RET" as described previously (23) with the following parameters included:

Total white blood cell count (WBC), total red blood cell count (RBC), platelet count (PLT), hemoglobin concentration (HGB), hematocrit (HCT), mean corpuscular volume (MCV), mean corpuscular hemoglobin content (MCH), mean corpuscular hemoglobin concentration (MCHC), red cell distribution width – coefficient of variance (RDW-CV), mean platelet volume (MPV), platelet distribution width (PDW), platelet large cell ratio (P-LCR), plateletcrit (PCT), absolute cell counts and proportions of WBC for lymphocytes (LYMPH), monocytes (MONO) as well as neutrophil (NEUT), eosinophil (EO) and basophil (BASO) granulocytes, and absolute cell counts and proportion of RDW of reticulocytes (RET), including proportions of reticulocyte maturation

states as determined by fluorescence intensity, mature low fluorescent reticulocytes (LFR), less mature medium fluorescent reticulocytes (MFR) and very immature highly fluorescent reticulocytes (HFR), as well as the sum of MFR and HFR as immature reticulocyte fraction (IRF).

Clinical chemistry analyses

Inorganic phosphate (Pi) was analyzed using an AU480 Clinical chemistry analyzer (Beckman-Coulter GmbH, Krefeld, Germany) and adapted test kits provided by Beckman Coulter in either undiluted or 1:2 with deionized water diluted EDTA-treated plasma samples as described previously (24). Heparinized capillaries were filled with 100 µL of whole blood and subjected to measurement of potassium and pH using a blood gas analyzer (ABL 835 Flex, Radiometer GmbH, Willich, Germany).

Blood pressure measurements

Blood pressure was measured continuously in male 10-12 week old C57BL/6 mice using an intra-arterial telemetric transmitter system as previously described (3). In brief, under isoflurane anesthesia a transmitter device (PhysioTel™ TA11PA-C10; Data Sciences International DSI, St. Paul, Minnesota, USA) was surgically implanted into the left common carotid artery one week prior to data sampling. The transmitter was placed subcutaneously over the abdominal area. All animals were then housed in open cages and allowed to recover for two weeks during which mice received unlimited access to regular chow (Ssniff, Soest, Germany) and tap water. Following recovery, the diet was changed to synthetic calcium-and oxalate-free diet (0% Ca 0% Oxalate, TD. 95027, Ssniff) for one week, followed by high oxalate diet (0% Ca 0.67% Oxalate,

TD. 95027, Ssniff) for 8 days and thereafter control diet for another 10 days. Blood pressure was detected and recorded continuously for 5 weeks by the Dataquest A.R.T. System (Data Sciences International DSI, St. Paul, Minnesota, USA). Systolic and diastolic blood pressure values were calculated as average of the last 24h-day of each diet period by the Dataquest ART 4.1 software (DSI). Mean arterial pressure (MAP) was calculated from diastolic and systolic pressure values using a standard equation.

Transcutaneous measurement of glomerular filtration rate (GFR) in conscious mice

For GFR measurement mice where anesthetized with isoflurane and a miniaturized imager device built from two light-emitting diodes, a photodiode and a battery (Mannheim Pharma & Diagnostics GmbH, Germany) was mounted via a double-sided adhesive tape onto the shaved animal's neck (26). For the duration of recording (approx. 1.5 h) each animal was conscious and kept in a single cage. Prior to the intravenous injection of 150 mg/kg FITC-sinistrin (Mannheim Pharma & Diagnostics GmbH, Germany), the skin's background signal was recorded for 5 min. After removing the imager device the data were analyzed using MPD Lab software (Mannheim Pharma & Diagnostics GmbH, Germany). The GFR [µl/min] was calculated from the decrease of fluorescence intensity over time (i.e. plasma half-life of FITC-sinistrin) using a two-compartment model, body weight of mouse and an empirical conversion factor (26).

Measurement of intact FGF23, PTH and phosphorus

The plasma concentration of intact FGF23 (Kainos Laboratories, Japan or Immutopics International, USA) and intact PTH (Immutopics International, USA) were measured by enzyme-

linked immunosorbent assays according to the manufacturers protocols. Phosphate was measured by the phosphomolybdate method (9, 10).

Magnetic resonance imaging (MRI)

Excised kidneys (n=12) from C57BL/6 male mice fed either high oxalate (n=6 kidneys) or control diet (n=6 kidneys) for 21 days were processed in 2% agarose and placed in a whole body coil for mice (Bruker, Ettlingen, Germany) of a dedicated small animal ultra-high-field MR scanner (ClinScan 7 Tesla, Bruker, Ettlingen, Germany). Standard sequences for morphology and mapping of T1-, T2- and T2*- relaxation times as well as of the apparent diffusion coefficient (ADC) (Siemens, Erlangen, Germany) were performed on kidneys in sagittal orientation (compare Fig. 5). By mapping of relaxation times, specific magnetic properties of tissues are quantified, which can be performed in multiple tissues and organs. Thereby an increase of T1 relaxation time may be associated with fibrosis, while prolonged T2 relaxation times are found in inflammation (25). Furthermore, calculation of the ADC by diffusion-weighted imaging captures the Brownian motion of water molecules that is locally altered in pathologic conditions like fibrosis, resulting in decreased water diffusion, and thus decreased ADC values (11). For post-processing of images, 3 regions of interest were placed in the cortex, medulla and transitional zone, respectively, to determine T1-, T2- and T2*- relaxation times as well as the ADC (Osirix, open-source software). Furthermore, the volume of the cortex was determined on morphological, T2 weighted images (Osirix, open-source software).

Histological examination of cardiac fibrosis

Hearts were excised, snap frozen in liquid nitrogen and stored at -80 °C until further use. The lower base of the left ventricle was embedded in tissue tec, whereupon 10 µm thick cross-sections were prepared on a SLEE-MNT cryostat (Mainz, Germany). Ventricular sections were stained for fibrotic tissue using Masson's trichrome staining (Sigma-Aldrich, Taufkirchen, Germany). Briefly, sections were fixed in 4% paraformaldehyde for 1 h at room temperature and refixed overnight in Bouin's solution. The next day, slides were washed in distilled water and incubated for 5 min with hematoxylin. After washing the slides in distilled water for 10 min, sections were incubated for 5 min in biebrich scarlet acid fuchsin. Slides were washed 3 times in distilled water, where after they were incubated in phosphomolybdic acid 3 times each for 3 min. After 5 min of incubation with aniline blue, which leads to a blue staining of fibrotic tissue, slides were rinsed in distilled water and dehydrated in isopropanol and xylene, before they were mounted with roti-histokit (Carl Roth, Karlsruhe, Germany). Differentiation was performed by incubating the slides 2 min in ice-cold acetic acid. After a washing step in distilled water, slides were covered with mounting medium. Microscopic composite images of the complete cross-sections were obtained at x150 magnification on a light microscope (Olympus IX70, Hamburg, Germany) with an inverted CCD-camera (Nikon DXM1200, Düsseldorf, Germany). Blue-stained fibrotic area was manually quantified by an observer blinded to the experimental condition on three cross-sections per heart using Image J software. The endocardium and trabeculae carnae were excluded from quantification. After determination of the ventricular area, the mean fibrosis content was calculated by dividing the area of Trichrome-stained fibrotic fibers by total left ventricular area. For qualitative electron microscopic investigations of the hearts several semithin and ultrathin sections were prepared and stained with methylene blue or uranyl

acetate/lead citrate, respectively. Images of ultrathin sections were taken with a Zeiss electron microscope LEO EM 910 (Zeiss, Oberkochen, Germany).

Preparation of femoral bones

Femoral bones were removed, weighed and fixed overnight using 1% (w/v) PFA buffered with PBS pH 7.4. Bones were decalcified in 10% (w/v) EDTA solution pH 7.4 before they were dehydrated and embedded in paraffin. Tissues were cut into 2-µm sections and stained with hematoxylin and eosin (H & E). Images were taken using BX60 Olympus microscope equipped with a XC 30 camera (Olympus BC, Hamburg, Germany).

Results

A diet high in soluble oxalate induces stable CKD

Previous work from our groups suggests that intraperitoneal oxalate can induce acute kidney injury (22), and a high oxalate diet can cause progressive renal failure (15). In the present study we first examined the effects of duration of feeding a soluble oxalate diet on renal function in C57BL/6 mice. Providing an oxalate diet induced a decline in GFR and an increase in plasma BUN and creatinine (Fig. 1A-C). Shorter duration of oxalate feeding followed by switching to control diet induced less advanced stages of CKD as defined by GFR, plasma BUN and creatinine (Fig. 1D-F). Serial monitoring documented that these parameters peaked at the end of oxalate feeding followed by mild recovery over the following 2 week period. Urinary oxalate increased following a switch to a soluble oxalate as compared to control diet (Fig. 1G) but no renal or bladder stones were detected (images not shown). Similarly, we observed a

sharp increase in plasma oxalate levels followed by a reduction of plasma oxalate levels when mice were switched back to control diet (Fig. 1H). Therefore, while a diet high in soluble oxalate was found to induce a progressive decline in renal function as previously reported (13), these results show for the first time that it can also be used to induce stable CKD after dietary oxalate is discontinued.

Renal pathology of oxalate-induced CKD

As progressive scarring and fibrotic processes are a hallmark of CKD irrespective of the initiating disease, we next examined renal histology of mice fed a soluble oxalate diet for various durations. Periodic acid-Schiff (PAS) staining revealed progressive tubular atrophy (Fig. 2A) resulting in remnant atubular glomeruli (Fig. 2B) (2, 17). In addition, infiltration by macrophages/monocytes and T cells was observed, mainly in areas of interstitial fibrosis (Fig. 3A). Furthermore, progressive renal fibrosis was demonstrated as measured by Collagen I, Silver and Trichrome staining, and the duration of feeding allowed titration of the degree of parenchymal loss (Fig. 3A). Expression profiling for markers of kidney injury, inflammation and fibrosis were consistent with progressive kidney atrophy (Fig. 3B). Female C57BL/6 mice revealed similar findings with very low inter-individual variability (Fig. 4A-F). Given the increasing use of diagnostic imaging modalities to assess changes of renal morphology, we performed magnetic resonance imaging (MRI) of kidneys from mice. As compared to mice receiving a control diet, animals receiving an oxalate diet displayed an increase in kidney cortex volume, T1-, T2- and T2*- relaxation times as well as a reduction of the apparent diffusion coefficient in the cortex (Fig 5). These significant differences in the cortex are known to be

associated with inflammation (increased volume and T2-time) and fibrosis (increased T1-time and decreased diffusion), and are consistent with findings from histology and expression profiling (25). Taken together, these data indicate that a high oxalate diet induces CKD in male and female C57BL/6 mice characterized by progressive kidney atrophy and fibrosis.

Oxalate-induced CKD in C57BL/6 mice demonstrates classical CKD complications

We next examined whether the mouse model displays human CKD complications. Oxalate diet induced normochromic anemia (Fig. 6A) without affecting other blood cell lines (Supplementary Table 1). CKD-related mineral bone disease (CKD-MBD) was demonstrated by elevated plasma FGF23 and PTH levels as well as hyperphosphatemia and hyperkalemia (Fig. 6B-E) in addition to metabolic acidosis (Fig. 6F). Bone marrow of femoral bones demonstrated no oxalate crystal deposition of mice receiving an oxalate diet (Fig. 6G). Furthermore, oxalate diet induced arterial hypertension (Fig. 7A and B), which persisted after cessation of the oxalate-rich diet (Fig. 7C and D). In addition, oxalate feeding induced cardiac fibrosis (Fig. 7E and F), another serious cardiovascular complication of CKD. Electron microscopy demonstrated fibroblast activation in mice receiving an oxalate diet, as demonstrated by an increase in size and vacuolization of fibroblasts as compared with mice receiving a control diet (Fig. 7G; white arrows). Similar to our observation in femoral bones, we could not detect any oxalate crystal deposition in heart tissue arguing against systemic oxalosis to explain the observed phenotype.

Thus, this model of oxalate diet-induced CKD presents with a wide spectrum of clinically established CKD complications.

283 It is of interest to compare the features of this oxalate-induced model of CKD with
284 previous models of CKD, as summarized in Table 2.
285
286 **Discussion**
287 The model of *unilateral ureteral obstruction (UUO)* has become a widely used model to
288 study CKD and fibrosis (3). While the model causes extensive parenchymal damage, functional
289 compensation by the intact contralateral kidney prevents a significant change of renal function
290 and the development of CKD complications (29). Absence of urine from the damaged kidney
291 precludes biomarker discovery studies. In contrast, the oxalate-diet induced CKD model enables
292 study of renal fibrosis while providing a functional endpoint of renal function as changes in GFR,
293 serum BUN and creatinine can be measured. It also allows the collection of urine and
294 demonstrates established CKD complications.
295 The *renal mass reduction models* have been a mainstay of CKD studies (16). Unilateral
296 nephrectomy is followed by either partial infarction or amputation of the poles of the remaining
297 kidney resulting in glomerular and tubule-interstitial injury. A strong limitation of the model is
298 the need for two surgical interventions requiring microsurgery training, confounding effects
299 related to anesthesia as well as surgical procedures, and the model's reproducibility and
300 variability (16). In addition, performing 5/6 nephrectomy limits the tissue available for analysis.
301 After 16 weeks, the C57BL/6 mice demonstrate increased albuminuria without increased blood
302 pressure and without developing cardiac fibrosis unless angiotensin II is administered (18). The
303 oxalate diet induced-model requires no microsurgery training/intervention, maintains sufficient
304 renal tissue for analysis, and reliably induces CKD complications.

The *adenine-induced model* of CKD - unlike UUO or renal mass reduction – does not require surgery. It has largely been established in rats (32) as it is not easily adapted to mice given their reluctance to consume adenine. Addition of casein appears to blunt the smell and taste of adenine in order to apply the approach to mice (13). Male mice present a more severe renal phenotype as compared with female mice presumably secondary to gender differences in the metabolism of adenine (7, 27). In addition, the model requires diets of different adenine content (13) or induction for 6 weeks (28). Most strikingly, the mice develop profound hypotension compared with mice receiving a control diet (19) In contrast, oxalate is readily eaten by mice; the amount of dietary intake can be precisely monitored by measuring urinary oxalate excretion. Additional benefits include the short time frame of 1-3 weeks for the induction of moderate to advanced CKD, which accelerates scientific work flow and reduces housing costs. Most strikingly, the oxalate model induces reliable and profound hypertension, an established complication of CKD in humans.

The *aristolochic acid model* represents an additional tool to investigate mechanisms of CKD progression and to access potential interventions (6, 12). Aristolochic acid I (AAI) is the active ingredient implicated in Chinese herb nephropathy. Intraperitoneal injection of AAI weekly has been shown to lead to progressive fibrosis and kidney failure that is more severe in male than female mice (6, 12), similar to observations made in the adenine model. No significant hypertension ensues (12). Contrary to the AAI model, the oxalate diet-induced model avoids direct handling and injections of mice. As the oxalate model works in male and female mice, it allows examination of gender differences in response to pharmaceutical interventions to treat CKD, providing a platform to use both male and female mice in preclinical studies as

requested by the National Institute of Health (4). In addition, gender-restricted models produce excess pups, which are avoided when both males and females can be used for experimentation, and the low inter-individual variability allows smaller group sizes.

The *folic acid nephropathy model* induces interstitial fibrosis following i.p. injection of high dosage of folic acid. The advantage of the model as compared with the UUO model is that renal function can be assessed. However, the model requires i.p. injections as compared with the oxalate feeding model, is somewhat variable and yet to be characterized in regards to gender differences and CKD complications (8, 30, 31).

Despite these advantages of the oxalate model over previous CKD models, a number of limitations have to be considered. Oxalate crystals primarily induce tubular injury (20-22), while many forms of human CKD are primarily driven by podocyte loss (5). The mechanism of crystal-induced progression may not translate to all forms of CKD. However, the extensively studied adenine and folic acid model are similarly crystal-induced (19). Likewise, one may argue that UUO as the benchmark model of fibrosis associated with an increase of vascular resistance and a reduced blood flow following surgery provides a mechanism of fibrosis not mimicking the pathophysiology of common forms of CKD (14).

Nevertheless, several elements of the oxalate model including tubular atrophy, renal inflammation, and fibrosis are common to many forms of CKD. In addition, one of the major strengths of the model is the reproducibility of CKD complications thereby allowing study of the mechanisms of FGF23 activation, hyperphosphatemia, hyperparathyroidism, hypertension and

cardiac fibrosis. Moreover, increasing the number of CKD models available may help to validate important findings and improve standards.

In conclusion, feeding a soluble oxalate diet represents a simple, reproducible and technically undemanding CKD model providing functional data in male as well as female C57BL/6 mice. Moreover, the duration of feeding enables titrated induction of various stages of CKD associated with numerous clinically important CKD complications. Thus, the oxalate diet-induced CKD model offers novel opportunities for CKD research.

Acknowledgements

This work was supported by grants from the Deutsche Forschungsgemeinschaft to HJA (AN372/16-1) and FK (KN 1148/2-1), by the German Federal Ministry of Education and Research (Infrafrontier grant 01KX1012) to MHA and the Interdisciplinary Center for Clinical Research (University Hospital Erlangen) and TRENAL program by the German Academic Exchange Service to VP. We thank Jana Mandelbaum, Dan Draganovic, Nada Cordasic, Sebastian Kaidel, Monika Klewer and Silvia Crowley for their expert technical assistance. Parts of this work were presented in the thesis project of J.E. at the Medical Faculty of the University of Munich.

Disclosure

The authors have nothing to disclose.

References

1. **Becker GJ and Hewitson TD.** Animal models of chronic kidney disease: useful but not perfect. *Nephrology, dialysis, transplantation : official publication of the European Dialysis and Transplant Association - European Renal Association* 28: 2432-2438, 2013.
2. **Chevalier RL and Forbes MS.** Generation and evolution of atubular glomeruli in the progression of renal disorders. *Journal of the American Society of Nephrology : JASN* 19: 197-206, 2008.
3. **Chevalier RL, Forbes MS, and Thornhill BA.** Ureteral obstruction as a model of renal interstitial fibrosis and obstructive nephropathy. *Kidney international* 75: 1145-1152, 2009.
4. **Clayton JA and Collins FS.** Policy: NIH to balance sex in cell and animal studies. *Nature* 509: 282-283, 2014.
5. **Collins AJ, Foley RN, Chavers B, Gilbertson D, Herzog C, Ishani A, Johansen K, Kasiske BL, Kutner N, Liu J, St Peter W, Guo H, Hu Y, Kats A, Li S, Li S, Maloney J, Roberts T, Skeans M, Snyder J, Solid C, Thompson B, Weinhandl E, Xiong H, Yusuf A, Zaun D, Arko C, Chen SC, Daniels F, Ebben J, Frazier E, Johnson R, Sheets D, Wang X, Forrest B, Berrini D, Constantini E, Everson S, Eggers P, and Agodoa L.** US Renal Data System 2013 Annual Data Report. *Am J Kidney Dis* 63: A7, 2014.
6. **Dai XY, Zhou L, Huang XR, Fu P, and Lan HY.** Smad7 protects against chronic aristolochic acid nephropathy in mice. *Oncotarget* 6: 11930-11944, 2015.
7. **Diwan V, Small D, Kauter K, Gobe GC, and Brown L.** Gender differences in adenine-induced chronic kidney disease and cardiovascular complications in rats. *American journal of physiology Renal physiology* 307: F1169-1178, 2014.
8. **Fink M, Henry M, and Tange JD.** Experimental folic acid nephropathy. *Pathology* 19: 143-149, 1987.
9. **Fiske CH and Subbarow Y.** The colorimetric determination of phosphorous. *The Journal of biological chemistry* 66: 375-400, 1925.
10. **Fiske CH and Subbarow Y.** The Nature of the "Inorganic Phosphate" in Voluntary Muscle. *Science* 65: 401-403, 1927.
11. **Hennedige T, Koh TS, Hartono S, Yan YY, Song IC, Zheng L, Lee WS, Rumpel H, Martarello L, Khoo JB, Koh DM, Chuang KH, and Thng CH.** Intravoxel incoherent imaging of renal fibrosis induced in a murine model of unilateral ureteral obstruction. *Magnetic resonance imaging* 33: 1324-1328, 2015.
12. **Huang L, Scarpellini A, Funck M, Verderio EA, and Johnson TS.** Development of a chronic kidney disease model in C57BL/6 mice with relevance to human pathology. *Nephron extra* 3: 12-29, 2013.
13. **Jia T, Olauson H, Lindberg K, Amin R, Edvardsson K, Lindholm B, Andersson G, Wernerson A, Sabbagh Y, Schiavi S, and Larsson TE.** A novel model of adenine-induced tubulointerstitial nephropathy in mice. *BMC nephrology* 14: 116, 2013.
14. **Kim W, Moon SO, Lee SY, Jang KY, Cho CH, Koh GY, Choi KS, Yoon KH, Sung MJ, Kim DH, Lee S, Kang KP, and Park SK.** COMP-angiopoietin-1 ameliorates renal fibrosis in a unilateral ureteral obstruction model. *Journal of the American Society of Nephrology : JASN* 17: 2474-2483, 2006.
15. **Knauf F, Asplin JR, Granja I, Schmidt IM, Moeckel GW, David RJ, Flavell RA, and Aronson PS.** NALP3-mediated inflammation is a principal cause of progressive renal failure in oxalate nephropathy. *Kidney international* 84: 895-901, 2013.
16. **Kren S and Hostetter TH.** The course of the remnant kidney model in mice. *Kidney international* 56: 333-337, 1999.
17. **Lech M, Grobmayr R, Ryu M, Lorenz G, Hartter I, Mulay SR, Susanti HE, Kobayashi KS, Flavell RA, and Anders HJ.** Macrophage phenotype controls long-term AKI outcomes--kidney regeneration versus atrophy. *Journal of the American Society of Nephrology : JASN* 25: 292-304, 2014.

18. **Leelahavanichkul A, Yan Q, Hu X, Eisner C, Huang Y, Chen R, Mizel D, Zhou H, Wright EC, Kopp JB, Schnermann J, Yuen PS, and Star RA.** Angiotensin II overcomes strain-dependent resistance of rapid CKD progression in a new remnant kidney mouse model. *Kidney international* 78: 1136-1153, 2010.
19. **Mishima E, Fukuda S, Shima H, Hirayama A, Akiyama Y, Takeuchi Y, Fukuda NN, Suzuki T, Suzuki C, Yuri A, Kikuchi K, Tomioka Y, Ito S, Soga T, and Abe T.** Alteration of the Intestinal Environment by Lubiprostone Is Associated with Amelioration of Adenine-Induced CKD. *Journal of the American Society of Nephrology : JASN* 26: 1787-1794, 2015.
20. **Mulay SR, Desai J, Kumar SV, Eberhard JN, Thomasova D, Romoli S, Grigorescu M, Kulkarni OP, Popper B, Vielhauer V, Zuchtriegel G, Reichel C, Bräsen JH, Romagnani P, Bilyy R, Munoz LE, Herrmann M, Liapis H, Krautwald S, Linkermann A, and Anders HJ.** Cytotoxicity of crystals involves RIPK3-MLKL-mediated necroptosis. *Nature Communications*: In press.
21. **Mulay SR, Evan A, and Anders HJ.** Molecular mechanisms of crystal-related kidney inflammation and injury. Implications for cholesterol embolism, crystalline nephropathies and kidney stone disease. *Nephrology, dialysis, transplantation : official publication of the European Dialysis and Transplant Association - European Renal Association* 29: 507-514, 2014.
22. **Mulay SR, Kulkarni OP, Rupanagudi KV, Migliorini A, Darisipudi MN, Vilaysane A, Muruve D, Shi Y, Munro F, Liapis H, and Anders HJ.** Calcium oxalate crystals induce renal inflammation by NLRP3-mediated IL-1beta secretion. *The Journal of clinical investigation* 123: 236-246, 2013.
23. **Rathkolb B, Fuchs H, Gailus-Durner V, Aigner B, Wolf E, and Hrabe de Angelis M.** Blood Collection from Mice and Hematological Analyses on Mouse Blood. *Current protocols in mouse biology* 3: 101-119, 2013.
24. **Rathkolb B, Hans W, Prehn C, Fuchs H, Gailus-Durner V, Aigner B, Adamski J, Wolf E, and Hrabe de Angelis M.** Clinical Chemistry and Other Laboratory Tests on Mouse Plasma or Serum. *Current protocols in mouse biology* 3: 69-100, 2013.
25. **Salerno M and Kramer CM.** Advances in parametric mapping with CMR imaging. *JACC Cardiovascular imaging* 6: 806-822, 2013.
26. **Schreiber A, Shulhevich Y, Geraci S, Hesser J, Stsepankou D, Neudecker S, Koenig S, Heinrich R, Hoecklin F, Pill J, Friedemann J, Schweda F, Gretz N, and Schock-Kusch D.** Transcutaneous measurement of renal function in conscious mice. *American journal of physiology Renal physiology* 303: F783-788, 2012.
27. **Stockelman MG, Lorenz JN, Smith FN, Boivin GP, Sahota A, Tischfield JA, and Stambrook PJ.** Chronic renal failure in a mouse model of human adenine phosphoribosyltransferase deficiency. *The American journal of physiology* 275: F154-163, 1998.
28. **Tanaka T, Doi K, Maeda-Mamiya R, Negishi K, Portilla D, Sugaya T, Fujita T, and Noiri E.** Urinary L-type fatty acid-binding protein can reflect renal tubulointerstitial injury. *The American journal of pathology* 174: 1203-1211, 2009.
29. **Ucero AC, Benito-Martin A, Izquierdo MC, Sanchez-Nino MD, Sanz AB, Ramos AM, Berzal S, Ruiz-Ortega M, Egido J, and Ortiz A.** Unilateral ureteral obstruction: beyond obstruction. *International urology and nephrology* 46: 765-776, 2014.
30. **Yang HC and Fogo AB.** Mechanisms of disease reversal in focal and segmental glomerulosclerosis. *Advances in chronic kidney disease* 21: 442-447, 2014.
31. **Yang HC, Zuo Y, and Fogo AB.** Models of chronic kidney disease. *Drug discovery today Disease models* 7: 13-19, 2010.
32. **Yokozawa T, Zheng PD, Oura H, and Koizumi F.** Animal model of adenine-induced chronic renal failure in rats. *Nephron* 44: 230-234, 1986.

460 **Figure legends**

461 **Figure 1. A diet high in soluble oxalate induces progressive or stable CKD.** A-C: C57BL/6 male
462 mice were fed either high oxalate or control diet for 21 days and (A) GFR, (B) plasma BUN, and
463 (C) plasma creatinine were measured at baseline, days 7, 14 and 21. D-F: C57BL/6 male mice
464 received high oxalate diet for 0, 7 or 14 days respectively and thereafter control diet for 14
465 days. (D) GFR, (E) plasma BUN, (F) plasma creatinine, (G) urine oxalate and (H) plasma oxalate
466 were measured at indicated time points. Data are mean ± SEM from 5 mice in each group.
467 *p<0.05, **p<0.01 and ***p<0.001 versus control group.

468

469 **Figure 2. Oxalate-induced CKD shows atubular glomeruli.** C57BL/6 male mice were fed either
470 high oxalate or control diet for 21 days. (A) PAS staining at various time points and
471 quantification, (B) Serial sections of the kidney were stained with Tetragonolobus lectin to
472 observe atubular glomeruli. Note the atubular glomerulus (clearly separated by a membrane) is
473 surrounded by tubules containing crystals. Data are mean ± SEM from 7-8 mice in each group.
474 **p<0.01 and ***p<0.001 versus control group.

475

476 **Figure 3. Pathology of oxalate-induced CKD in male mice.** C57BL/6 male mice were fed either
477 high oxalate or control diet for 21 days. (A) F4/80, CD3, Collagen I, Silver, Masson Trichrome
478 staining and their quantification, (B) Gene expression of kidney injury (TIMP-2, Kim-1),
479 inflammation (RANTES, TNFα, IL-6) and fibrosis (Fibronectin, FSP-1, Col1a1) was analyzed using
480 RT-PCR at different time points. Data are mean ± SEM from 7-8 mice in each group. *p<0.05,

**p<0.01 and ***p<0.001 versus control group. $^{+}$p<0.05, $^{++}$p<0.01 and $^{+++}$p<0.001 versus control group. $^{\#\#}$p<0.01 and $^{\#\#\#}$p<0.001 versus control group.

Figure 4. Oxalate-induced CKD in female mice. C57BL/6 female mice were fed either high oxalate or control diet for 21 days. Note that female mice develop comparable CKD to male mice. (A) Plasma BUN levels. (B) Plasma creatinine levels. (C) Quantification of tubular injury. (D) Quantification of CD3+ve cells. (E) Quantification of CaOx crystal deposits, F4/80+ve macrophages, Masson Trichrome, Silver and Collagen I+ve area. (F) mRNA expression of kidney injury markers, pro-inflammatory genes and pro-fibrotic genes. Data are mean ± SEM from 7-8 mice in each group. *p<0.05, **p<0.01 and ***p<0.001 versus control group.

Figure 5. Magnetic resonance imaging (MRI) of oxalate-induced CKD. MRI was performed on kidneys of C57BL/6 male mice fed either high oxalate or control diet for 21 days. (A, B) On representative morphological images, contrast characteristics of kidneys in the cortex, medulla and transitional zone could be visualized. (C) Quantitative parameters on total cortex volume, (D) T1 - relaxation time, (E) T2 - relaxation time, (F) T2* - relaxation time and (G) Apparent diffusion coefficient (ADC) showed significant differences between the groups in cortex, medulla or transitional zone. C, cortex; M, medulla; CM, transitional zone. Data are mean ± SEM from 7-8 mice in each group. *p<0.05, **p<0.01 and ***p<0.001 versus control group.

Figure 6. Oxalate-induced CKD demonstrates classical CKD complications. A-F: C57BL/6 male mice were fed either high oxalate or control diet for 21 days and different parameters for CKD

503 complications were analyzed. (A) Hemoglobin levels in blood. (B) Plasma FGF-23 levels. (C)
504 Plasma parathyroid hormone levels. (D) Plasma phosphorous levels. (E) Plasma potassium levels
505 (F). pH of blood. (G) HE staining of femoral bones. Data are mean ± SEM from 4-5 mice in each
506 group. *p<0.05, **p<0.01 and ***p<0.001 versus control group.
507
508 **Figure 7. Oxalate-induced CKD demonstrates hypertension and cardiac fibrosis.** (A) Mean
509 arterial blood pressure. (B) Heart Rate. C-D: C57Bl6 male mice received high oxalate diet for 8
510 days and thereafter control diet for 10 days. (C) Mean arterial blood pressure. (D) Heart Rate. E-
511 F: Cardiac fibrosis was quantified (E) on Masson trichrome staining of heart cross-sections (F) at
512 day 21 after high oxalate diet. (G) Electron microscopy of heart sections. Data are mean ± SEM
513 from 4-5 mice in each group except for n=2 at day 18 (control diet fed group) in C-D. *p<0.05,
514 **p<0.01 and ***p<0.001 versus control group.
515

516

517 **Table 1.** Primers sequences

Target		Primer sequence
KIM1	Forward	5’-TCAGCTCGGGAATGCACAA -3’
	Reverse	5’-TGGTTGCCTTCCGTGTCTCT -3’
TIMP2	Forward	5`-CAGACGTAGTGATCAGAGCCAAA -3`
	Reverse	5`-ACTCGATGTCTTTGTCAGGTCC -3`
RANTES	Forward	5’- GTGCCCACGTCAAGGAGTAT-3’
	Reverse	5’- CCACTTCTTCTCTGGGTTGG-3’
IL 6	Forward	5’- TGATGCACTTGCAGAAAACA -3’
	Reverse	5’- ACCAGAGGAAATTTTCAATAGGC - 3’
Fibronectin	Forward	5’-GGAGTGGCACTGTCAACCTC - 3’
	Reverse	5’-ACTGGATGGGGTGGGAAT - 3’
Collagen1a1	Forward	5’-ACATGTTCAGCTTTGTGGACC -3’
	Reverse	5’-TAGGCCATTGTGTATGCAGC- 3’
FSP-1	Forward	5’- CAGCACTTCCTCTCTCTTGG -3’
	Reverse	5’-TTTGTGGAAGGTGGACACAA - 3’
TNF-alpha	Forward	5’- CCACCACGCTCTTCTGTCTAC -3’
	Reverse	5’-AGGGTCTGGGCCATAGAACT - 3’
Alpha-SMA	Forward	5’- ACTGGGACGACATGGAAAAG-3’
	Reverse	5’- GTTCAGTGGTGCCTCTGTCA- 3’
iNOS	Forward	5’- GAGACAGGGAAGTCTGAAGCAC-3’
	Reverse	5’- CCAGCAGTAGTTGCTCCTCTTC-3’
18s RNA	Forward	5’- GCAATTATTCCCCATGAACG-3’
	Reverse	5’- AGGGCCTCACTAAACCATCC- 3’

Table 2: Comparison of murine CKD models.

CKD Animal Models	1	2	3	4	5	6	7	8	References
Unilateral ureteral obstruction (UUO)	✓	✓	✓	-	✓	-	-	-	(3, 29)
Surgical renal mass ablation (5/6 Nephrectomy)	✓	✓	-	-	✓	-	-	✓	(16, 18)
Adenine-induced CKD	✓	✓	-	✓	-	✓	✓	-	(7, 13, 19, 27, 28, 32)
Aristolochic acid-induced CKD	✓	✓	✓	✓	-	✓	✓	-	(6, 12)
Folic acid-induced CKD	✓	-	-	✓	?	✓	✓	?	(8, 30, 31)
Oxalate-induced CKD	✓	✓	✓	✓	✓	✓	✓	✓	

Criteria

1. Inducible in C57BL/6 mice
2. Reliable induction of stable CKD
3. Require relatively short time to induce CKD and, thus, limit the burden for animals, reduce housing costs
4. Avoid surgical interventions, thus, minimize animal distress and use of painkillers
5. Inducible in male and female mice with low inter-individual variability
6. Avoid reduction in renal mass
7. Reduction in GFR
8. CKD complications such as normochromic anemia, hyperphosphatemia, hyperparathyroidism, hyperkalemia, acidosis, hypertension, and cardiovascular disease.

Figure 1

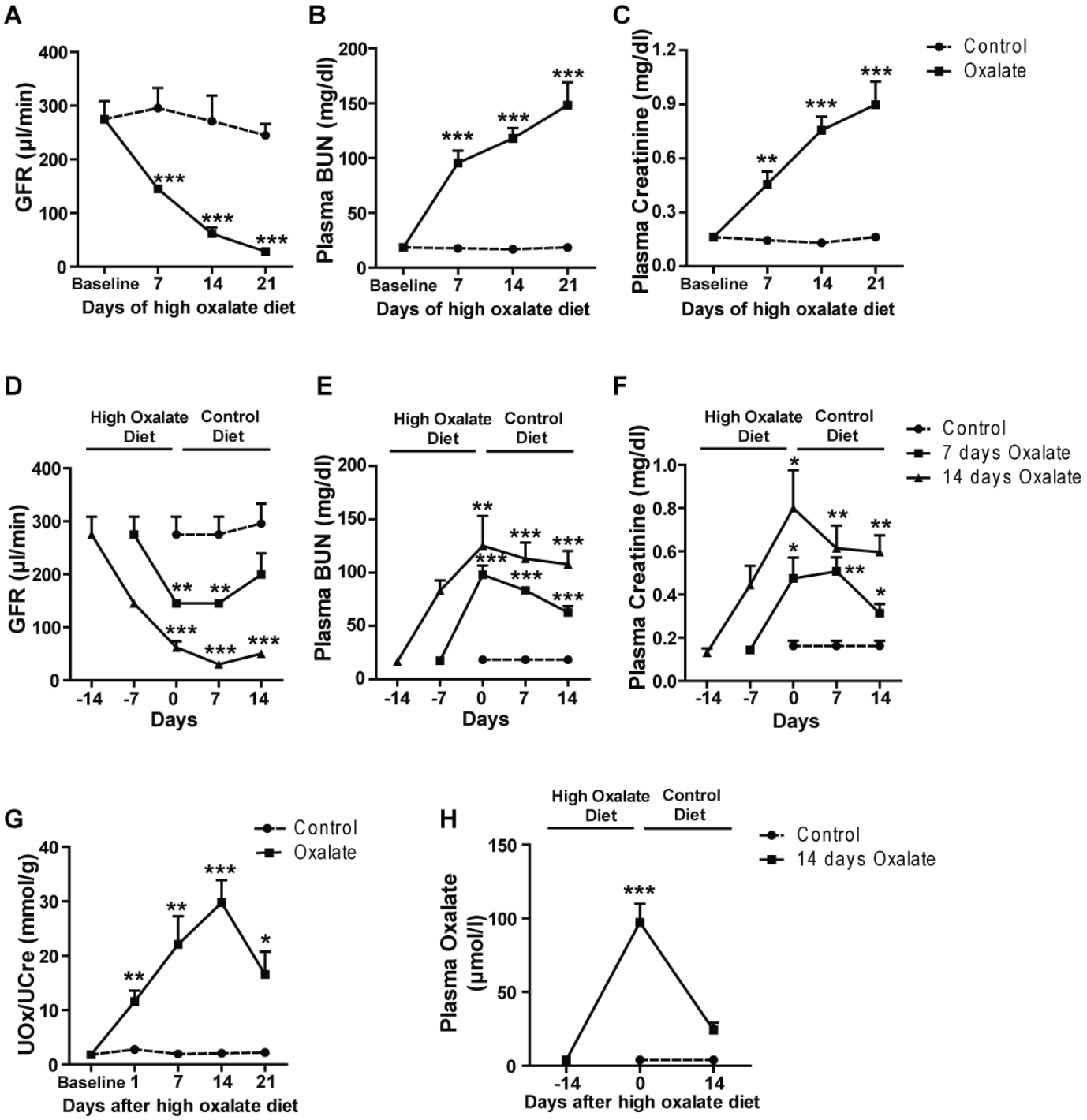
A
GFR (µl/min)
Baseline 7 14 21
Days of high oxalate diet
B
Plasma BUN (mg/dl)
Baseline 7 14 21
Days of high oxalate diet
C
Plasma Creatinine (mg/dl)
Baseline 7 14 21
Days of high oxalate diet
Control
Oxalate
D
High Oxalate Diet
Control Diet
GFR (µl/min)
-14 -7 0 7 14
Days
E
High Oxalate Diet
Control Diet
Plasma BUN (mg/dl)
-14 -7 0 7 14
Days
F
High Oxalate Diet
Control Diet
Plasma Creatinine (mg/dl)
-14 -7 0 7 14
Days
Control
7 days Oxalate
14 days Oxalate
G
UOx/UCre (mmol/g)
Baseline 1 7 14 21
Days after high oxalate diet
Control
Oxalate
H
High Oxalate Diet
Control Diet
Plasma Oxalate (µmol/l)
-14 0 14
Days after high oxalate diet
Control
14 days Oxalate

Figure 2

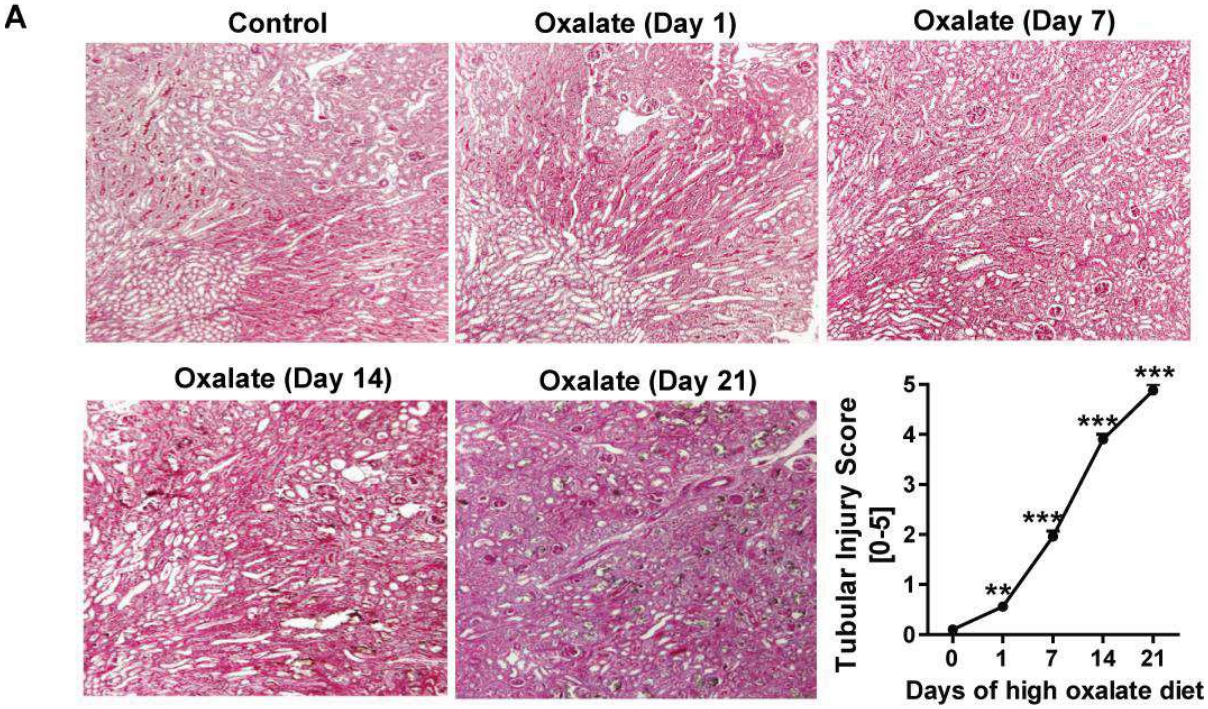
A
Control
Oxalate (Day 1)
Oxalate (Day 7)
Oxalate (Day 14)
Oxalate (Day 21)
Tubular Injury Score [0-5]
Days of high oxalate diet
0
1
7
14
21
**
***
***
***

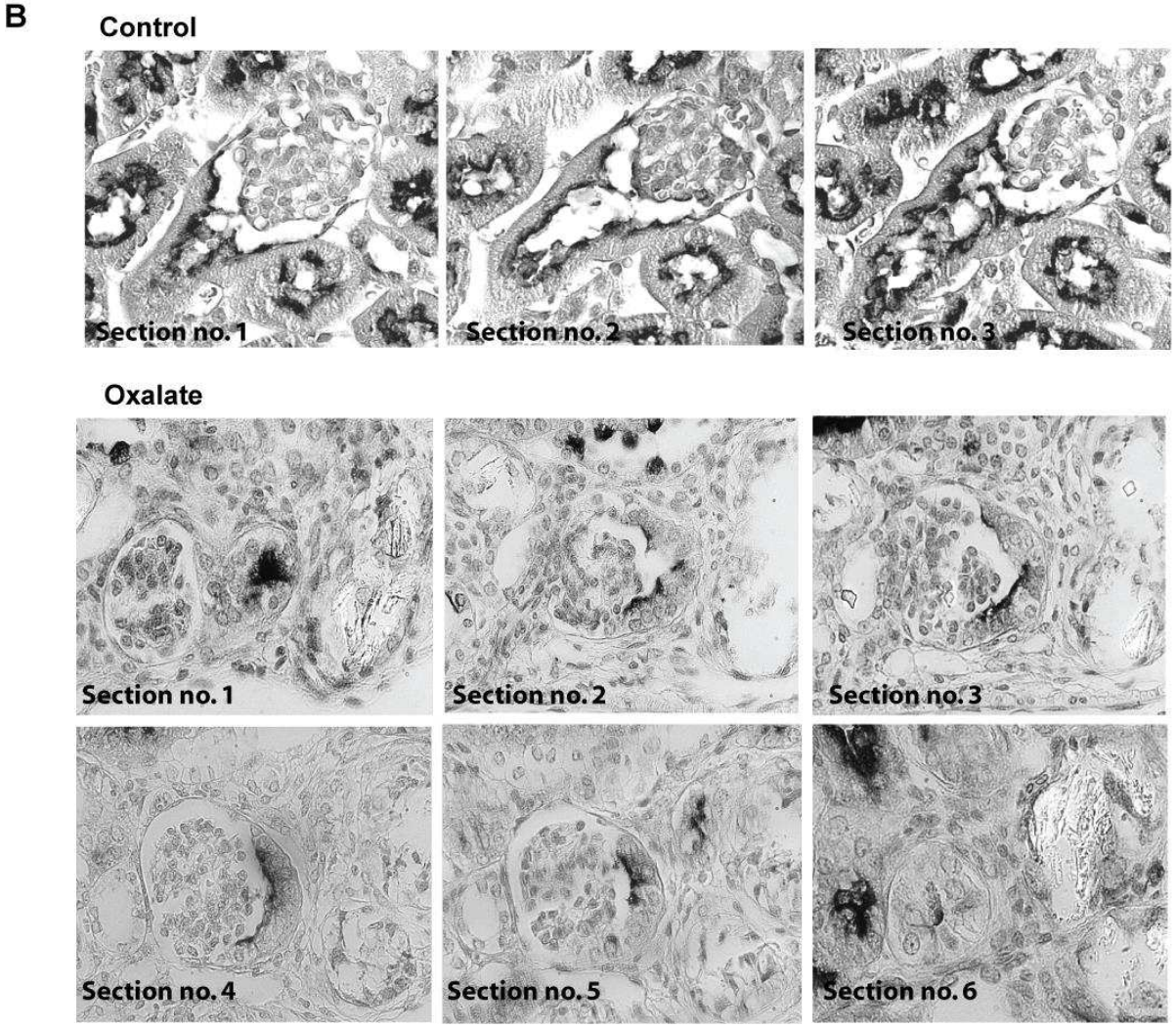
B
Control
Section no. 1
Section no. 2
Section no. 3
Oxalate
Section no. 1
Section no. 2
Section no. 3
Section no. 4
Section no. 5
Section no. 6

Figure 3

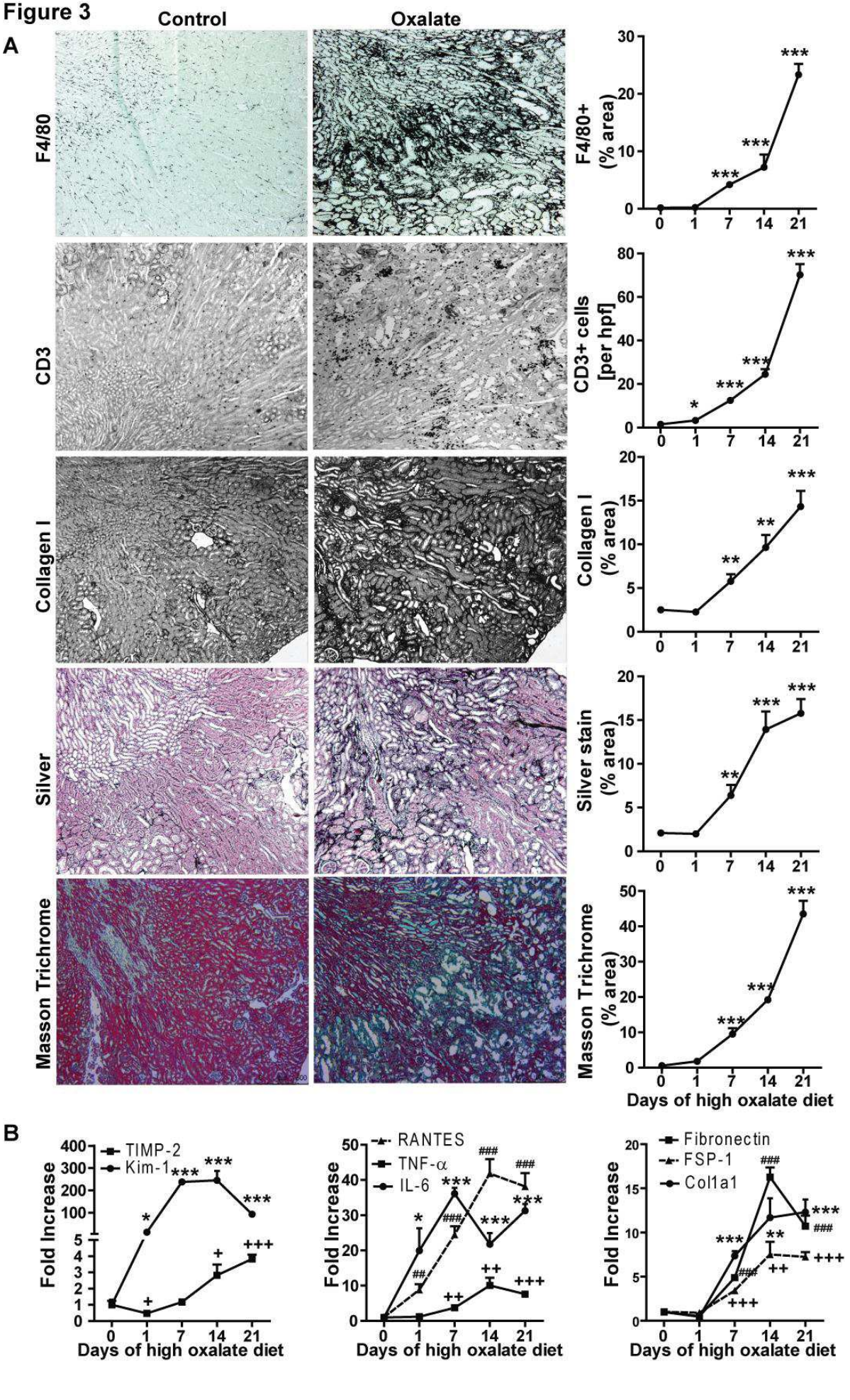
A
Control
Oxalate
F4/80
CD3
Collagen I
Silver
Masson Trichrome
F4/80+ (% area)
CD3+ cells [per hpf]
Collagen I (% area)
Silver stain (% area)
Masson Trichrome (% area)
Days of high oxalate diet
B
TIMP-2
Kim-1
Fold Increase
Days of high oxalate diet
RANTES
TNF-α
IL-6
Fold Increase
Days of high oxalate diet
Fibronectin
FSP-1
Col1a1
Fold Increase
Days of high oxalate diet

Figure 4

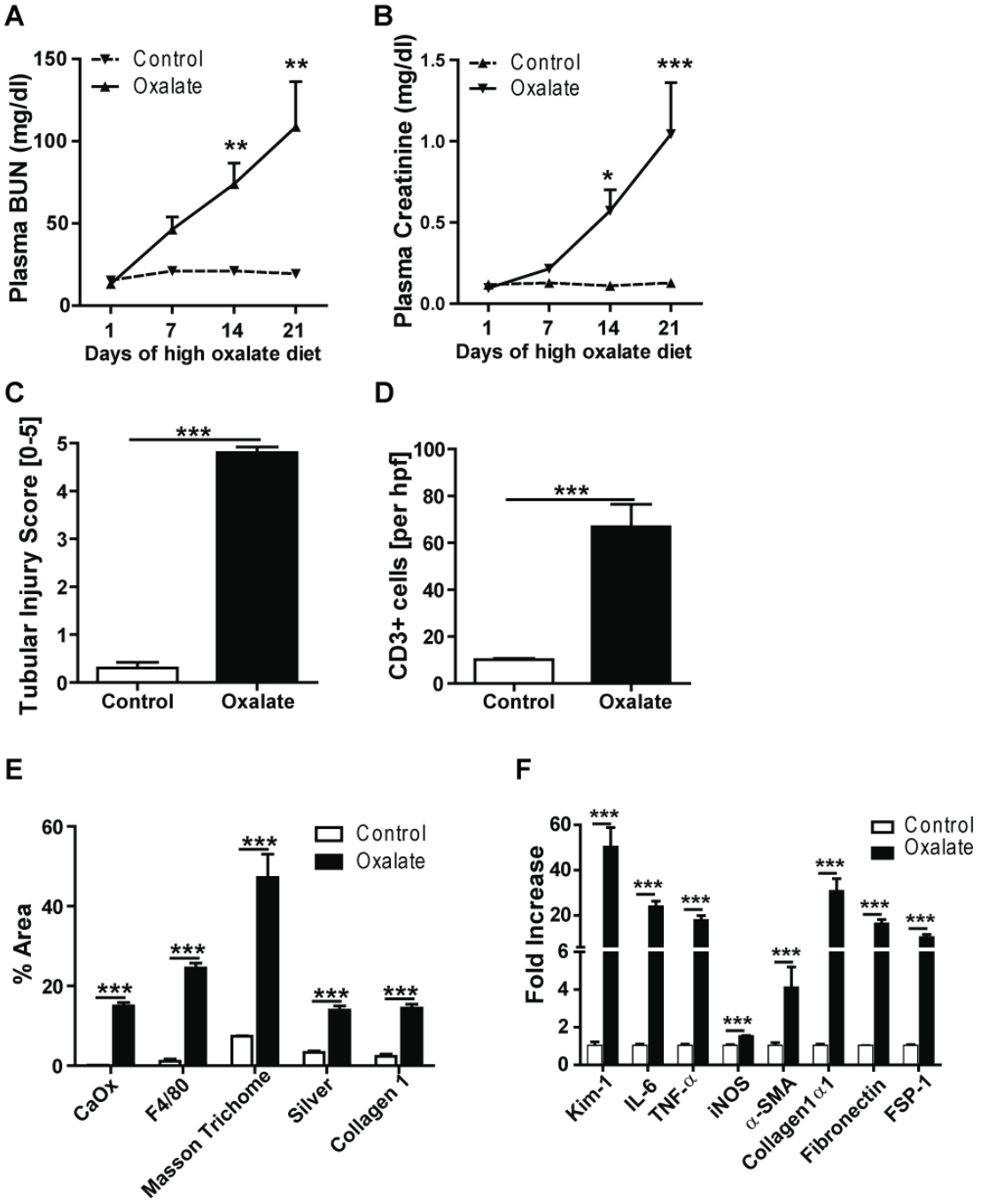
A
Plasma BUN (mg/dl)
Control
Oxalate
Days of high oxalate diet
B
Plasma Creatinine (mg/dl)
Control
Oxalate
Days of high oxalate diet
C
Tubular Injury Score [0-5]
Control
Oxalate
D
CD3+ cells [per hpf]
Control
Oxalate
E
% Area
Control
Oxalate
CaOx
F4/80
Masson Trichome
Silver
Collagen 1
F
Fold Increase
Control
Oxalate
Kim-1
IL-6
TNF-α
iNOS
α-SMA
Collagen1α1
Fibronectin
FSP-1

Figure 5

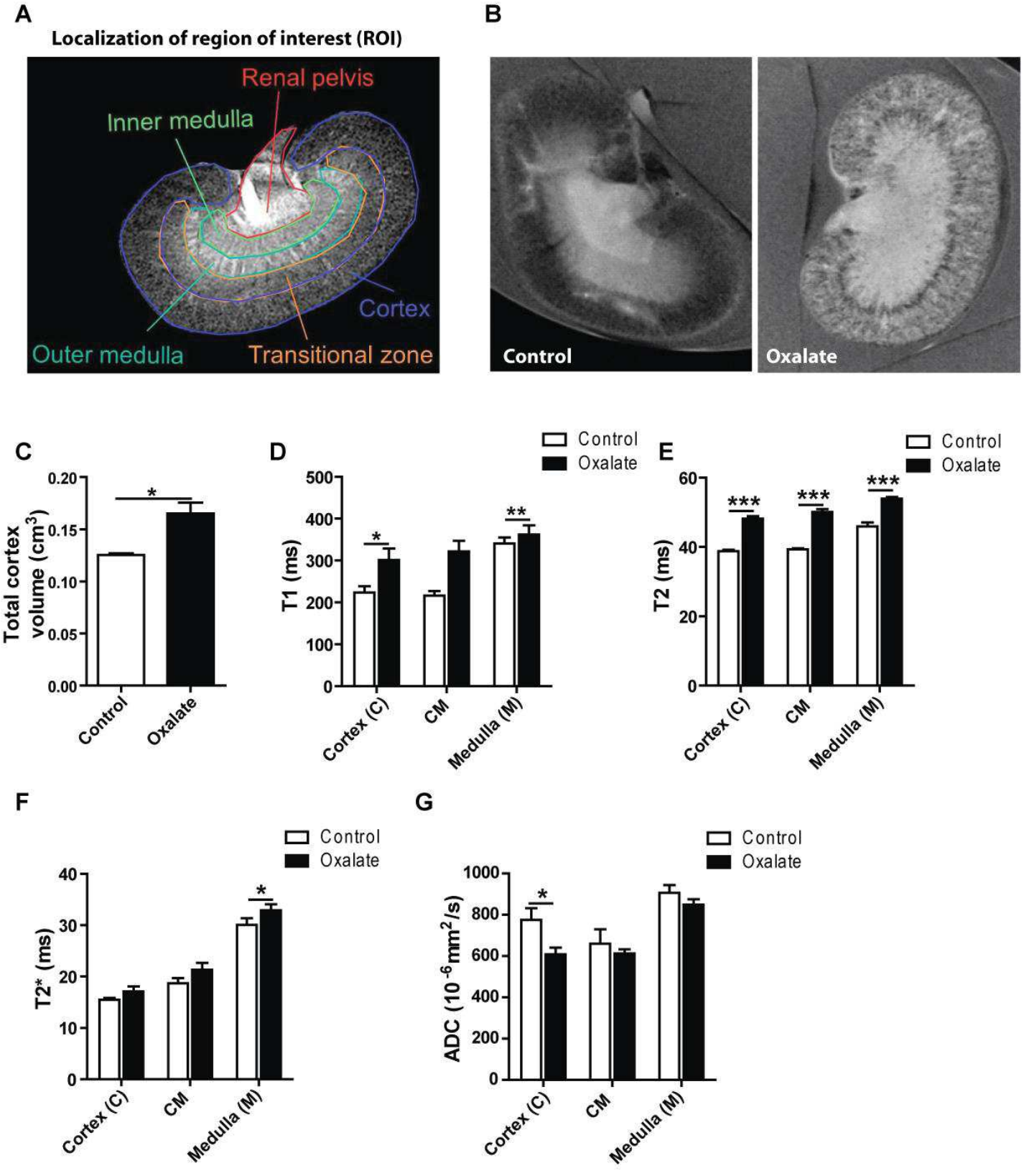
A
Localization of region of interest (ROI)
Renal pelvis
Inner medulla
Cortex
Outer medulla
Transitional zone
B
Control
Oxalate
C
Total cortex volume (cm3)
0.20
0.15
0.10
0.05
0.00
*
Control
Oxalate
D
Control
Oxalate
T1 (ms)
500
400
300
200
100
0
*
**
Cortex (C)
CM
Medulla (M)
E
Control
Oxalate
T2 (ms)
60
40
20
0
***
***
***
Cortex (C)
CM
Medulla (M)
F
Control
Oxalate
T2* (ms)
40
30
20
10
0
*
Cortex (C)
CM
Medulla (M)
G
Control
Oxalate
ADC (10-6mm2/s)
1000
800
600
400
200
0
*
Cortex (C)
CM
Medulla (M)

Figure 6

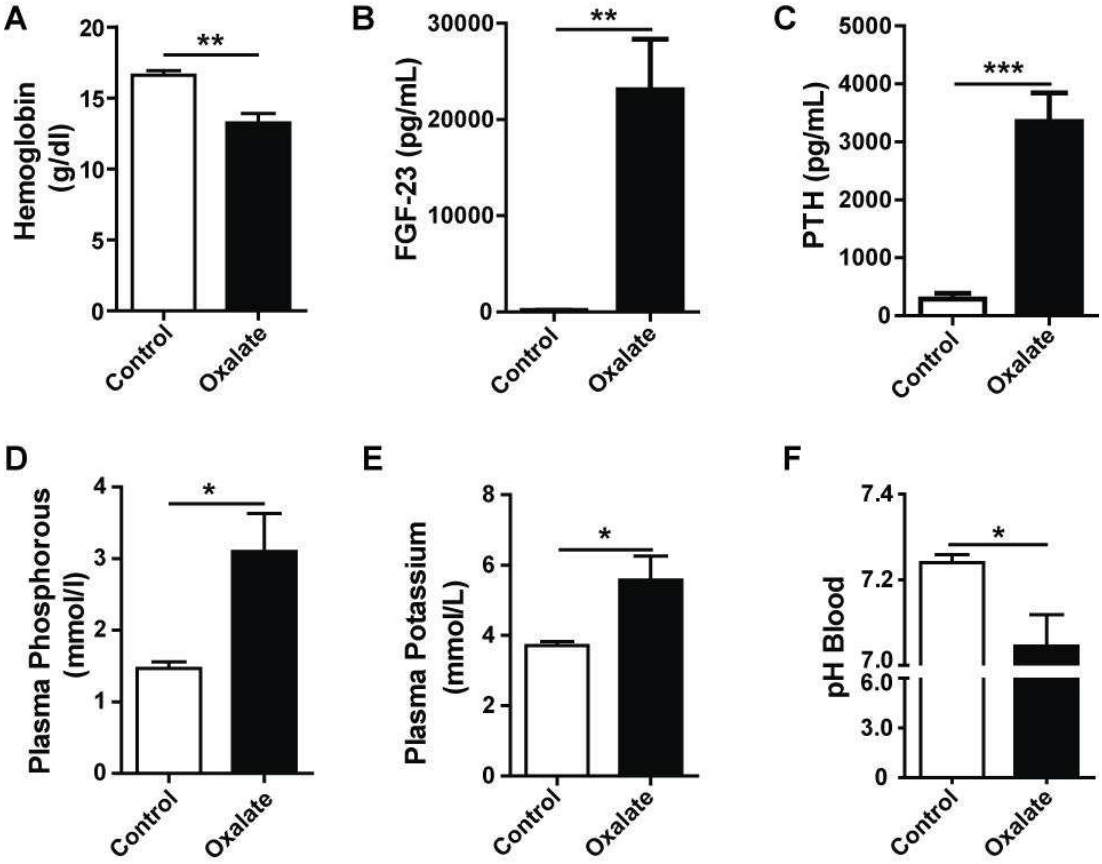
A
Hemoglobin (g/dl)
20
15
10
5
0
**
Control
Oxalate
B
FGF-23 (pg/mL)
30000
20000
10000
0
**
Control
Oxalate
C
PTH (pg/mL)
5000
4000
3000
2000
1000
0
***
Control
Oxalate
D
Plasma Phosphorous (mmol/l)
4
3
2
1
0
*
Control
Oxalate
E
Plasma Potassium (mmol/L)
8
6
4
2
0
*
Control
Oxalate
F
pH Blood
7.4
7.2
7.0
6.0
3.0
0
*
Control
Oxalate

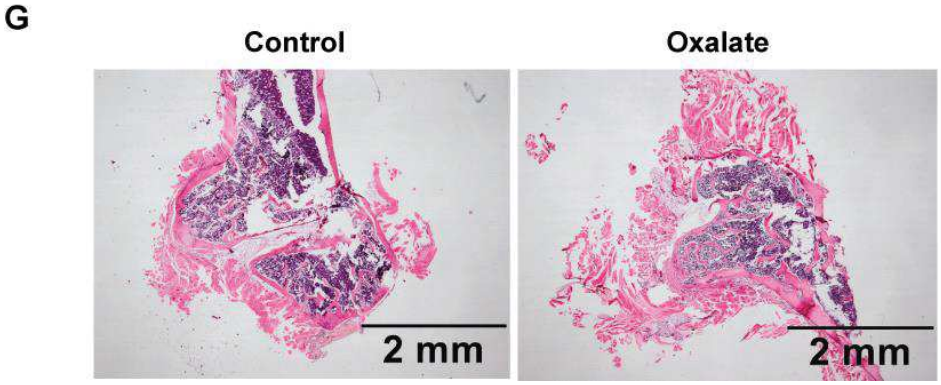
G
Control
Oxalate
2 mm
2 mm

Figure 7

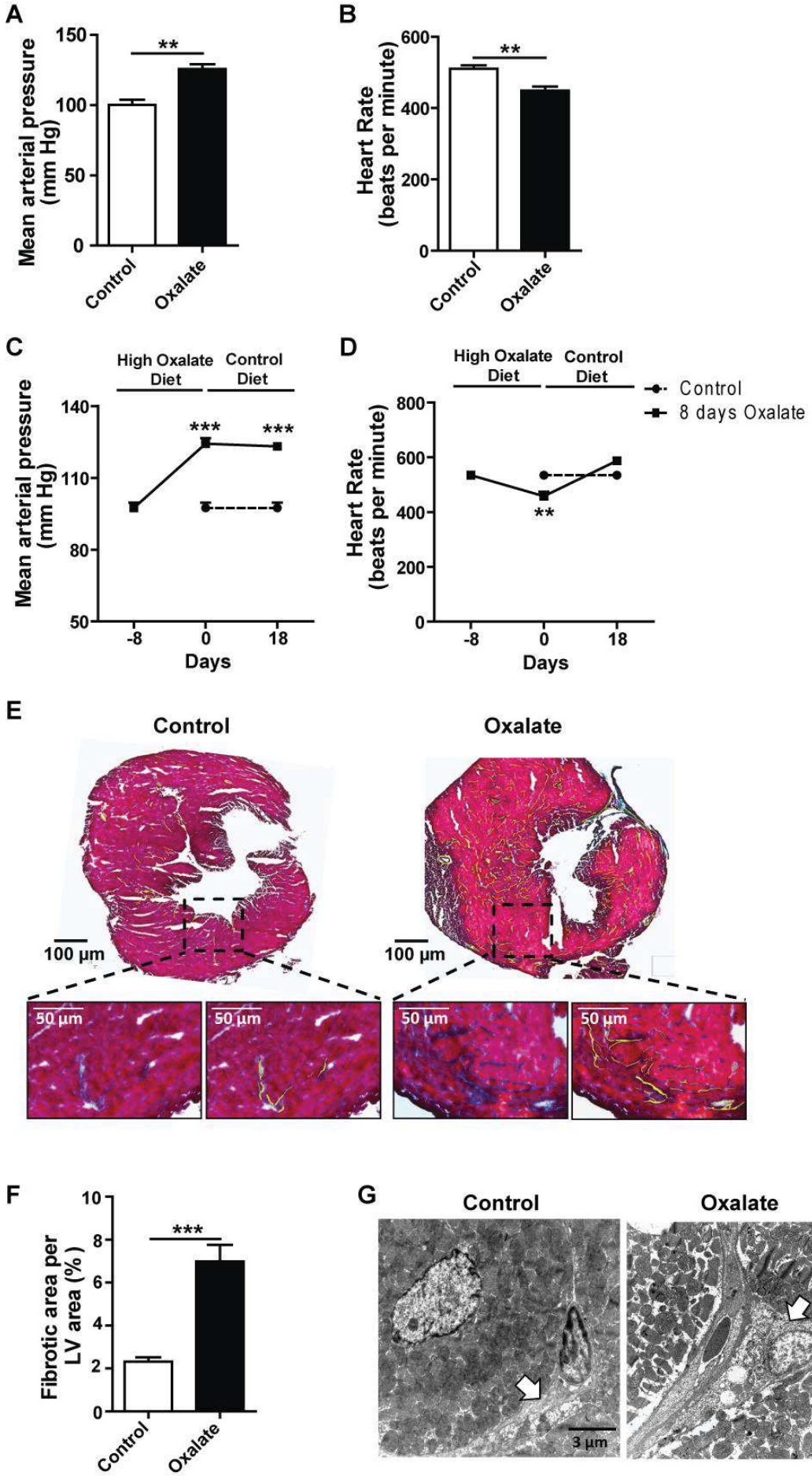
A
Mean arterial pressure (mm Hg)
150
100
50
0
**
Control
Oxalate
B
Heart Rate (beats per minute)
600
400
200
0
**
Control
Oxalate
C
High Oxalate Diet
Control Diet
Mean arterial pressure (mm Hg)
140
110
80
50
***
***
-8
0
18
Days
D
High Oxalate Diet
Control Diet
Control
8 days Oxalate
Heart Rate (beats per minute)
800
600
400
200
0
**
-8
0
18
Days
E
Control
Oxalate
100 µm
100 µm
50 µm
50 µm
50 µm
50 µm
F
Fibrotic area per LV area (%)
10
8
6
4
2
0
***
Control
Oxalate
G
Control
Oxalate
3 µm
3 µm